Journal of Biomedical Optics

BiomedicalOptics.SPIEDigitalLibrary.org

Evaluation of transdermal delivery of nanoemulsions in *ex vivo* porcine skin using two-photon microscopy and confocal laser-scanning microscopy

Sanghoon Choi
Jin Woong Kim
Yong Joong Lee
Thomas Delmas
Changhwan Kim
Soyeun Park
Ho Lee

SPIE.

Evaluation of transdermal delivery of nanoemulsions in *ex vivo* porcine skin using two-photon microscopy and confocal laser-scanning microscopy

Sanghoon Choi,[a] Jin Woong Kim,[b,c] Yong Joong Lee,[a] Thomas Delmas,[d] Changhwan Kim,[a] Soyeun Park,[e,*] and Ho Lee[a,*]
[a]Kyungpook National University, College of Engineering, School of Mechanical Engineering, 80 Daehak-ro Buk-gu, Daegu 702-701, Republic of Korea
[b]Hanyang University, Department of Applied Chemistry, 55 Hanyangdaehak-ro, Sangnok-gu, Ansan 426-791, Republic of Korea
[c]Hanyang University, Department of Bionano Technology, 55 Hanyangdaehak-ro, Sangnok-gu, Ansan, 426-791, Republic of Korea
[d]Capsum SAS, Heliopolis Batiment C, 3 allée des Maraichers, 13013 Marseille, France
[e]Keimyung University, College of Pharmacy, 1095 Dalgubeol-daero Dalseo-gu, Daegu 704-701, Republic of Korea

Abstract. This study experimentally evaluates the self-targeting ability of asiaticoside-loaded nanoemulsions compared with nontargeted nanoemulsions in *ex vivo* experiments with porcine skin samples. Homebuilt two-photon and confocal laser-scanning microscopes were employed to noninvasively examine the transdermal delivery of two distinct nanoemulsions. Prior to the application of nanoemulsions, we noninvasively observed the morphology of porcine skin using two-photon microscopy. We have successfully visualized the distributions of the targeted and nontargeted nanoemulsions absorbed into the porcine skin samples. Asiaticoside-loaded nanoemulsions showed an improved *ex vivo* transdermal delivery through the stratum corneum compared with nonloaded nanoemulsions. As a secondary measure, nanoemulsions-applied samples were sliced in the depth direction with a surgical knife in order to obtain the complete depth-direction distribution profile of Nile red fluorescence. XZ images demonstrated that asiaticoside-loaded nanoemulsion penetrated deeper into the skin compared with nontargeted nanoemulsions. The basal layer boundary is clearly visible in the case of the asiaticoside-loaded skin sample. These results reaffirm the feasibility of using self-targeting ligands to improve permeation through the skin barrier for cosmetics and topical drug applications. [DOI: 10.1117/1.JBO.19.10.106006]

Keywords: transdermal delivery; nanoemulsions; two-photon microscopy; confocal laser scanning microscopy.

Paper 140483RR received Jul. 25, 2014; revised manuscript received Sep. 11, 2014; accepted for publication Sep. 11, 2014; published online Oct. 9, 2014.

1 Introduction

The organ most exposed to the external environment is skin. Skin has many functions including but not limited to heat exchange, tactile sensation, water and electrolyte leakage prevention, immune function, and synthesis of vitamin D. The skin is largely composed of three layers: the epidermis, the dermis, and the subcutaneous layer. The epidermis is the outermost layer directly exposed to the external environment and provides the first line of defense against external stimulants. It consists mainly of keratinocytes but also contains melanocytes, Langerhans cells, Merkel cells, and inflammatory cells. Among its diverse functions, the single most important function of the skin is the protection against ultraviolet rays, micro-organisms, and chemicals to minimize their effects on the body. While the protection the epidermis provides has many positive benefits against undesirable stimulants, it can also hinder the delivery of drugs or other topically applied treatment chemicals deeper into the skin. For this reason, the topical application of drugs is often limited or ineffective,[1,2] and much of topical medication and cosmetics research has focused on improving the delivery of active ingredients through the epidermis.

There are many techniques for improving the epidermal permeability of drugs, e.g., massaging,[3] ultrasonic agitation,[4,5] laser treatment,[6,7] microneedles,[8,9] and emulsions.[10] Among these methods, the use of emulsions for improving transdermal delivery has been attracting more interest recently due to low cost, ease of preparation, excellent skin affinity, and stability. An emulsion is broadly defined as a mixture of two or more immiscible liquids. More specific to drug delivery, one liquid is dispersed throughout another liquid in the form of small droplets in an emulsion. Since relatively large micron-sized droplets tend to flocculate and coalesce into larger droplets, nanoemulsions whose drop sizes are less than hundreds of nanometers have been both theoretically and experimentally investigated in order to prevent such irreversible destabilization.[11] Nanoemulsions not only have a better penetrating ability compared with micro- or macroemulsions due to small droplet sizes, but can also target specific cells by incorporating various ligands in the droplets. Such targeting ability of droplets within nanoemulsions can be exploited in targeted tumor therapy[12,13] or topical application of drugs targeting specific cells in the skin. There are several methods for fabricating nanoemulsions, including high-pressure homogenization,[14,15] ultrasonic emulsification,[16–18] phase inversion temperature method,[19–21] solvent

*Address all correspondence to: Soyeun Park and Ho Lee, E-mail: sypark20@kmu.ac.kr and holee@knu.ac.kr

0091-3286/2014/$25.00

Table 1 Nanoemulsion compositions.

Nanoemulsion designation	Ingredients	w/w % of the dispersed phase	w/w %
F50 NC50 (control, no asiaticoside-loading)	Saline solution (phosphate buffered solution)	—	99.00
	Myrj s40 (PEG-40 Stearate)	46.0	0.46
	Semisynthetic glycerides	22.7	0.23
	Soybean oil (Glycine soja oil)	22.7	0.23
	Soybean lecithin (lecithin)	8.7	0.09
	Nile red	0.01	0
F50A (asiaticoside-loaded)	Saline solution (phosphate buffered solution)	—	99.00
	Myrj s40 (PEG-40 Stearate)	44.0	0.46
	Semisynthetic glycerides	23.0	0.23
	Soybean oil (Glycine soja oil)	23.0	0.23
	Soybean lecithin (lecithin)	9.0	0.09
	Centella asiatica	1.0	0.01
	Nile red	0.01	0

displacement method,[22,23] and phase inversion composition method,[24,25] and there has been a steady increase in the number of reported studies on the application of nanoemulsions to various areas, including drug delivery, cosmetics, and food sciences.

Recently, our group has investigated the benefits of self-assembled nanoemulsions incorporating ligands for targeting specific skin cells.[12] In that study, nanoemulsions with droplet sizes ranging from 20 to 150 nm with palmitoyl-lysine-threonine-threonine-lysine-serine (palmitoyl-KTTKS) and asiaticoside ligands were prepared and evaluated for stability and cytotoxicity. Nanoemulsions with two different ligands as well as the control nanoemulsion with no ligand were applied *in vitro* to human dermal fibroblasts (HDFa) and keratinocytes from the HaCaT cell lines,[26] and their targeting abilities were assessed by adhesion assay. Nile red fluorescence signatures indicated that palmitoyl-KTTKS-loaded nanoemulsions preferentially adhered to dermal fibroblast cells, while asiaticoside-loaded nanoemulsions showed an increased level of binding to keratinocytes. However, improved *in vitro* adherence does not automatically guarantee the same result in *in vivo* or *ex vivo* conditions since transdermal delivery of nanoemulsions could be highly dependent on the physical and chemical properties of skin.

In this study, we extend the previous work on *in vitro* evaluation of asiaticoside-targeted nanoemulsions to investigate the targeting effectiveness of the same nanoemulsion in *ex vivo* porcine skin samples. First, images of *ex vivo* porcine skin samples were acquired with two-photon microscopy in order to obtain the structural information. Then, the self-targeted

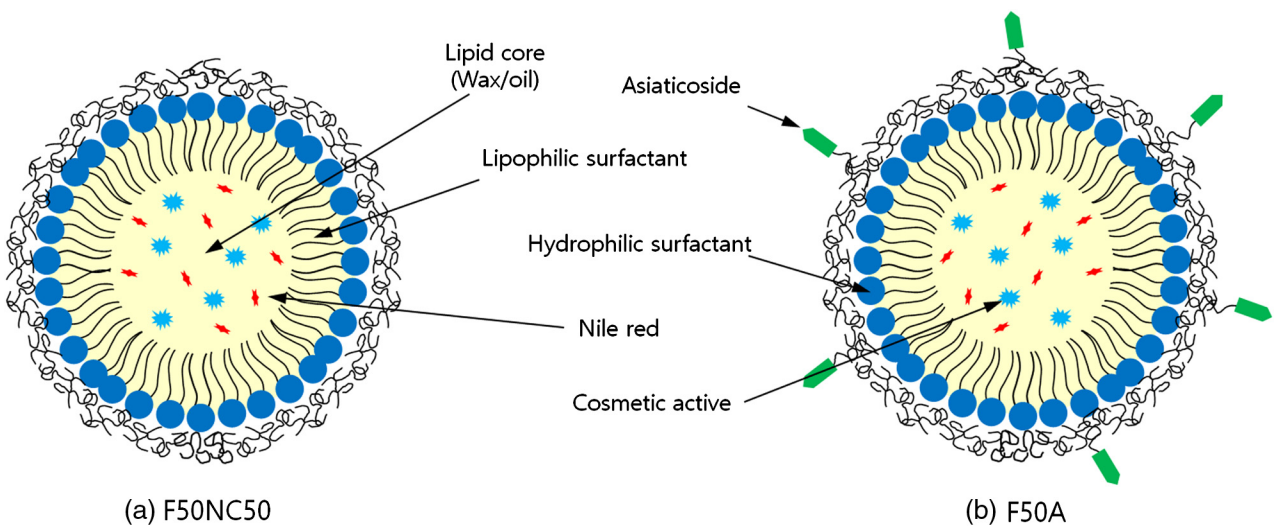

Fig. 1 Schematic representation of nanoemulsion compositions. (a) F50A and (b) F50NC50.

(asiaticoside-loaded) and nontargeted (control) nanoemulsions were applied to the porcine skin samples, and their *ex vivo* distributions were observed using confocal laser scanning microscopy (CLSM). Independently acquired structural information of skin and the distribution of targeted and nontargeted nanoemulsions in *ex vivo* measurements would allow a more complete picture for transdermal delivery of nanoemulsions and their effectiveness in targeting specific skin cells.

2 Methodology

2.1 *Specific Cell Targeted Nanoemulsion Preparation*

Nanoemulsions used in the experiments were prepared following the process published elsewhere (summarized in Table 1).[12] In short, lipophilic and hydrophilic phases were separately prepared and roughly homogenized at 45°C. After roughly mixing the two phases at 45°C, ultrasonication was performed for 5 min to obtain nanoemulsions with an average nanodroplet size of 50 nm. The size of the nanoemulsion was chosen based on our previous study, in which nanoemulsions with 50-nm droplets exhibited slightly more Nile red fluorescence in the epidermis than 120-nm droplet-containing nanoemulsions. In order to achieve the targeted delivery of nanoemulsions, the incorporation of a specific ligand, asiaticoside, was utilized (Fig. 1). Asiaticoside is a trisaccharide pentacyclic triterpene typically extracted from Centella asiatica, an herbaceous, annual plant natively found in the wetlands in Asia. Although the increased adhesion of asiaticoside targeted nanoemulsion to keratinocytes is not currently fully understood, an interaction between triterpenoids and keratinocyte cells is believed to be the key for such an effect.[11]

2.2 *Ex Vivo Porcine Skin Preparation*

Figure 2 shows the general procedure for preparing porcine skin samples for two-photon and confocal laser scanning microscopy measurements.

Fresh porcine skin was supplied from a local slaughterhouse. Upon arrival, porcine skin was cut into patches of 2×2 cm^2 in size and prepared for experiments within 6 h of slaughter. Typical porcine skin samples contained both the epidermis and the dermis. In order to prevent dehydration of the skin samples during the course of measurements, paper tissue soaked with a sufficient amount of phosphate-buffered saline (PBS) 1X was placed under the skin samples. It was confirmed beforehand that the tissue paper did not contain any fluorescent material. 0.5 μl of F50NC50 and F50A nanoemulsions were topically drop-applied to the porcine skin samples using pipettes. In order to minimize the damage to the skin samples, no physical contact was made during the application of the nanoemulsion using a pipette. Then, the Petri dish containing the porcine skin samples was covered with a sheet of aluminum foil in order to block the ambient light, and the samples treated with F50NC50 and F50A nanoemulsions were kept at room temperature for 30 h to allow the nanoemulsions to permeate into the skin. Finally, the skin samples were carefully washed with flowing PBS to remove the access nanoemulsions from the skin after 30 h of treatment followed by drying with clean tissue paper. The epidermal side of the skin sample was covered with a cover glass (150 μm thickness) for two-photon and confocal laser scanning microscopy imaging.

2.3 *Two-Photon Microscopy and Confocal Laser Scanning Microscopy*

The microscopy setup used in this study is schematically illustrated in Fig. 3. Both two-photon and CLSM systems are homebuilt and share the same scanning optics and objective lens. For the excitation sources, a mode-locked Ti:sapphire femtosecond laser with a center wavelength of 730 nm was used to excite autofluorescence in the porcine skin for two-photon microscopy, while a continuous-wave Ar/Kr laser with a wavelength of 532 nm was used for Nile red fluorescence in the confocal channel. A 40× water immersion objective lens with the numerical aperture of 1.2 was used for collecting backscattered and fluorescent light from the skin samples. The combination of a polygonal scanning mirror and a galvanometer was set to give 30 image frames per second. The autofluorescence and Nile red fluorescence were detected by two separate photomultiplier tubes (PMTs). The long-pass dichroic mirror with the

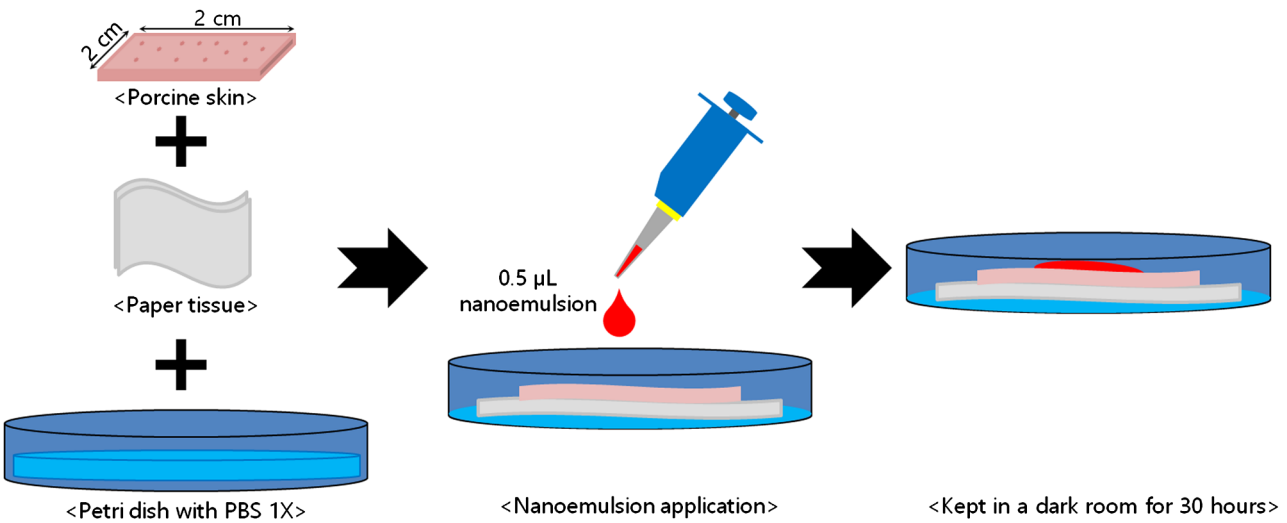

Fig. 2 Procedures for preparing porcine skin samples for microscopy measurements. Fresh porcine skin was cut into 2×2 cm^2 patches and imaged by two-photon microscopy. Then the samples were treated with nanoemulsions, F50A, and F50NC50 for 30 h for confocal fluorescence microscopy.

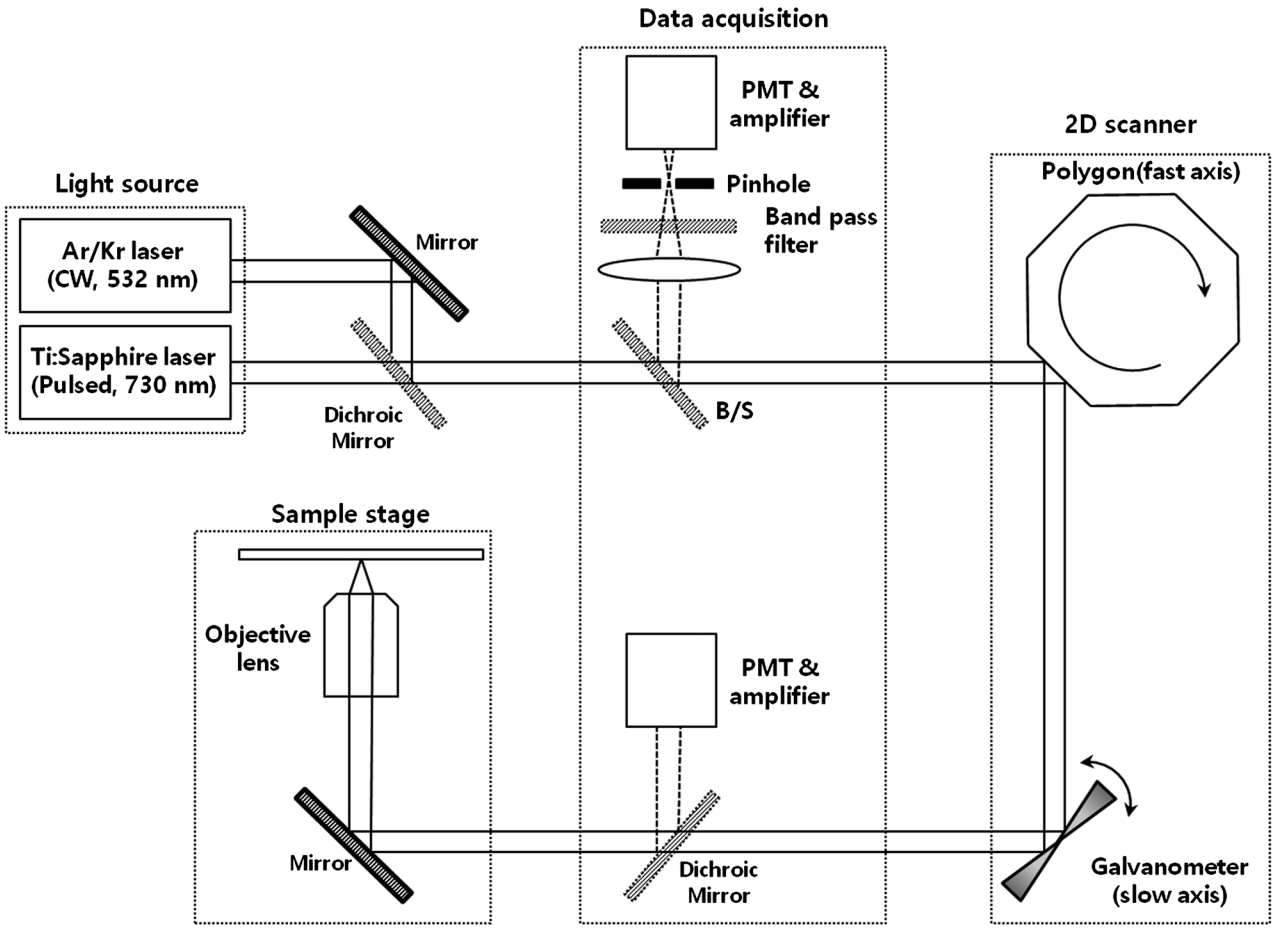

Fig. 3 Schematic of two-photon and confocal scanning laser microscopy setup. Both two-photon microscopy and confocal microscopy share the same scanning optics, while laser sources and detection photomultiplier tubes are different. The homebuilt setup allows a fast and easy switching between imaging modes without a major alteration in the setup.

edge wavelength of 658.8 nm (Di02-R635-25x36, Semrock Inc.) in front of the PMT responsible for measuring autofluorescence prevented backscattered 532-nm laser beam from entering the PMT. Nile red fluorescence was detected in a confocal configuration through a band pass filter with a pass band of 580 to 620 nm (FF01-600/37-25, Semrock Inc.) and a pinhole with a diameter of 50 μm. The signals from the PMTs were digitized with a frame grabber to produce snapshot images or movie streams. The axial resolution corresponding to the axial thickness of one image plane for two-photon microscopy was ~1 μm, while that for CLSM was experimentally found to be ~4 μm. Unless otherwise stated, the field of view was set to 300×300 μm^2 (500×500 pixels) for image acquisition.

3 Results and Discussion

Prior to the application of nanoemulsions, we noninvasively observed the morphology of porcine skin using two-photon microscopy. Skin samples were placed on an automated z-axis translation stage and the stack of *en face* images of untreated skin were taken every 1 μm in the direction of depth from the surface. Figure 4 shows autofluorescence images of a porcine skin sample obtained by two-photon microscopy in the depth direction before the application of nanoemulsions. The numbers in the parenthesis indicate the depths from the surface. The stratum corneum [Fig. 4(a)] was observed up to a few microns from the surface. The stratum granulosum [Fig. 4(b)] and the stratum spinosum [Fig. 4(c)] were observed from 20 to 50 μm in depth.

Clearly visible individual skin cells producing bright autofluorescence aided the identification of the stratum granulosum and the stratum spinosum. The extracellular boundaries and nuclei of the cell appeared darker than the cytoplasm due to weaker autofluorescence. Figure 4(d) presents the *en face* image of the epidermal and dermal junction where the basal layer and the papillary dermis layer coexist. Multiple basal cell layers appear as circles in the image (indicated as arrows), and the upper dermal layer can be observed inside the circles. The papillary basal layer and the upper dermis can coexist at the same depth due to the papillary nature of the basal layer. The papillary basal layer is more clearly visualized in the B-scanned image [XZ image in the plane perpendicular to the skin surface, Fig. 4(e)]. The papillary shaped basal layer, which defines the boundary between the epidermis and dermis (indicated as arrows), was clearly distinguished. A total of nine different spots were chosen and their subsurface morphologies were imaged and investigated. In terms of various skin structures and their depths from the surface, all nine locations displayed similar structure-depth results.

After visually verifying the morphology of the porcine skin samples, two types (F50A and F50NC50) of nanoemulsions

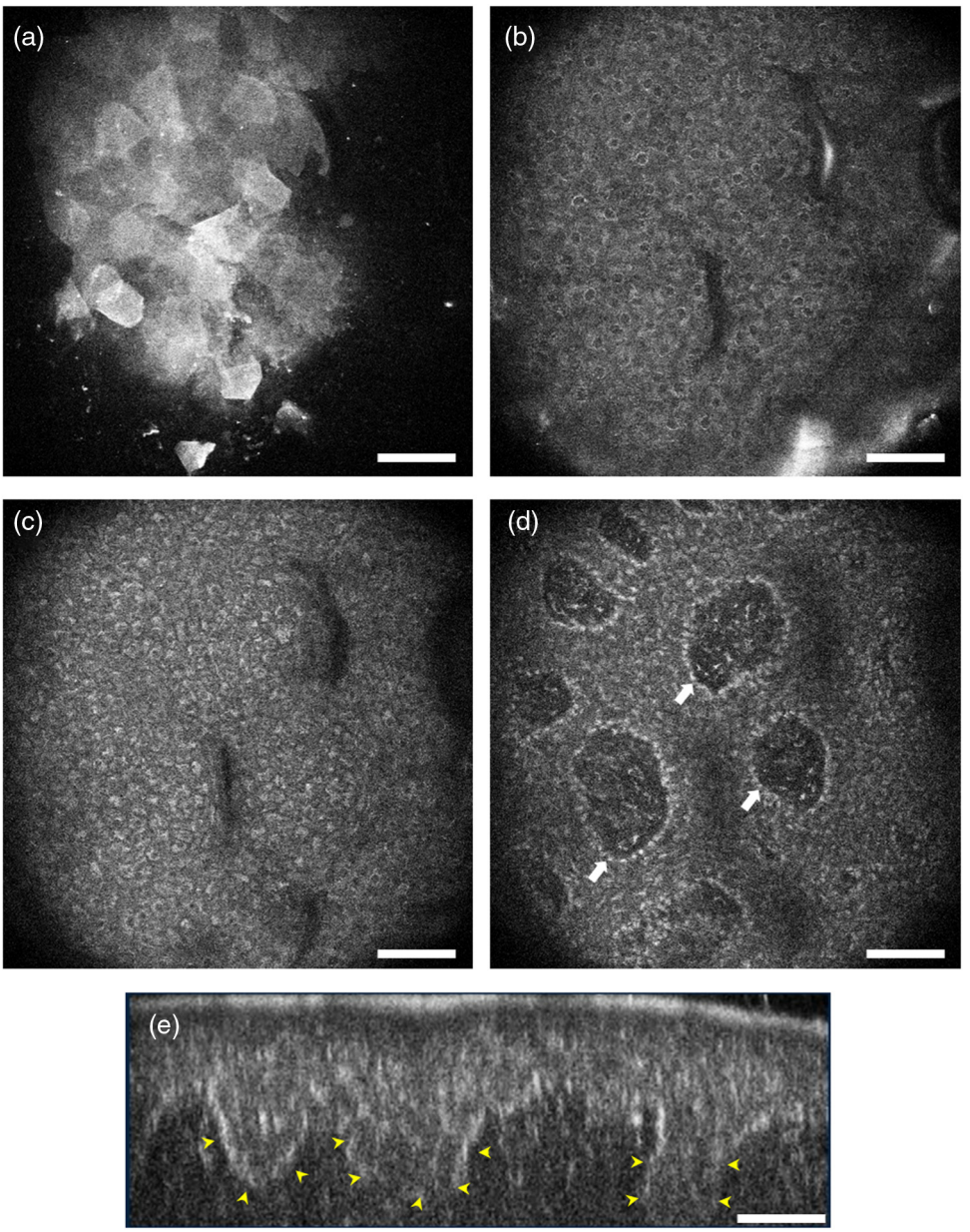

Fig. 4 Autofluorescence images of a porcine skin sample showing different skin structures at different depths. (a) Stratum corneum (surface), (b) stratum granulosum (20 μm), (c) stratum spinosum (40 μm), (d) stratum basal (60 μm), and (e) XZ image. Arrows indicate the basal layer. Scale bars are 50 μm.

were applied to the samples as discussed in Sec. 2.2 and Nile red fluorescence images were taken by CLSM. Figure 5 shows typical Nile red fluorescence images from porcine skin samples treated with F50A and F50NC50. The power of the excitation laser and the amplification factor for the PMTs were adjusted identically during the image acquisition process for two distinct nanoemulsions. Asiaticoside is believed to selectively target rhamnose binding lecithins, and previous *in vitro* studies found that asiaticoside targeted nanoemulsions significantly enhanced the colocalization of Nile red fluorescence signals with keratinocyte cells.[12] Nile red fluorescence intensity is correlated with the density of the corresponding nanoemulsions in images shown in Fig. 5.

When comparing the images shown in Fig. 5, it is clearly evident that F50A penetrated deeper into the skin than F50NC50. For all observed samples, Nile red fluorescence was detected down to ~30 to 40 μm and up to 100 μm below the surface for F50NC50 samples and F50A samples, respectively. While Nile red fluorescence signals from F50A nanoemulsion were observed from the skin surface down to the dermis, Nile red fluorescence signals from F50NC50 were observed mainly in the stratum corneum. Although Nile red fluorescence from F50NC50 nanoemulsion was detected in the stratum granulosum, the signal level was near the detection limit of the PMT used in the experiment.

In order to visualize the distribution of the applied nanoemulsions, three-dimensional reconstruction was performed using the stack of *en face* images with a rendering software (Image J, National Institutes of Health, USA). Figure 6 shows how F50A and F50NC50 are distributed in the skin samples under investigation. For all images in Fig. 6, the full-scale lengths were 300 μm for both x and y axes and 100 μm for

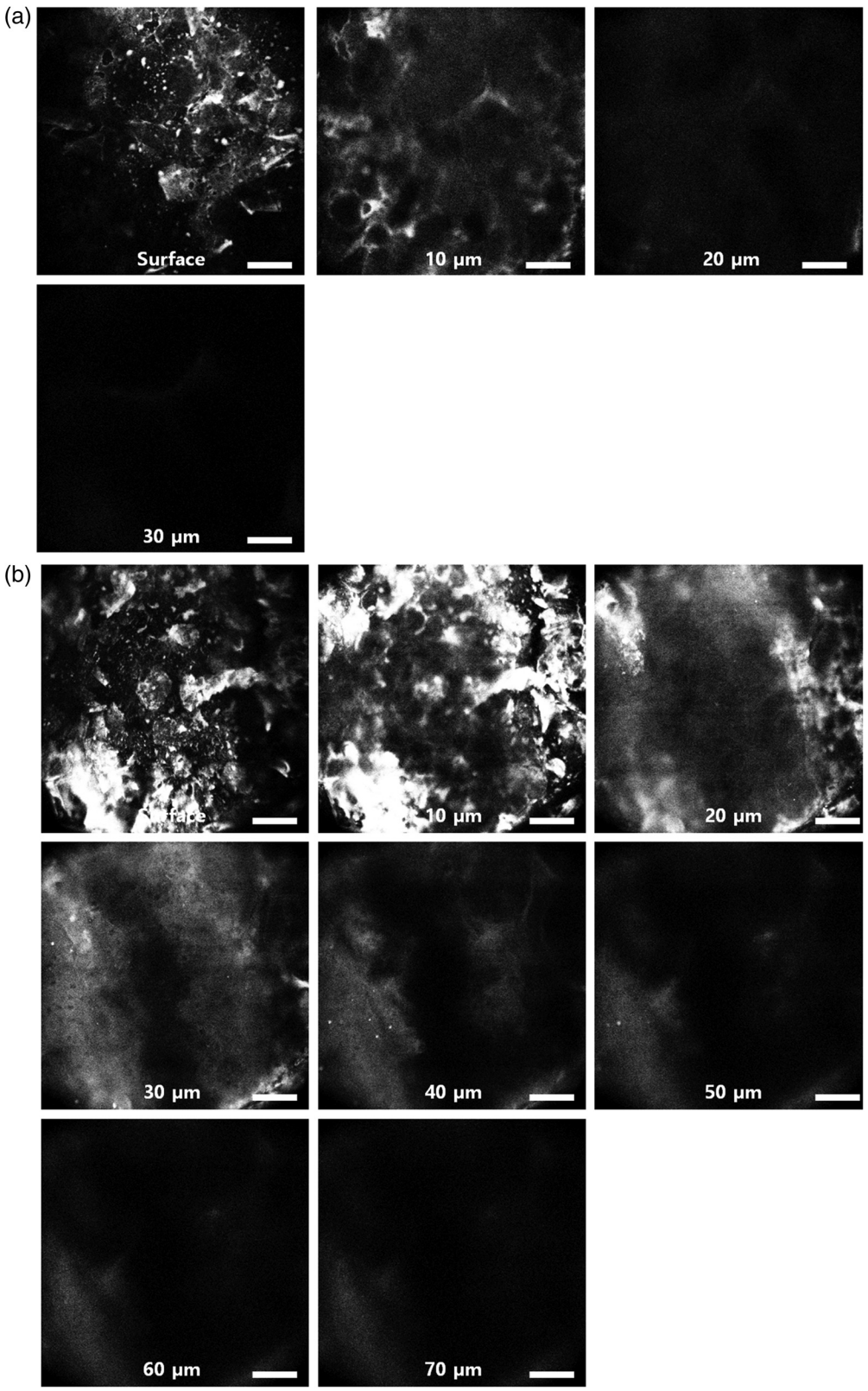

Fig. 5 Nile red fluorescence images from the porcine skin sample treated with (a) F50NC50 and (b) F50A in 10-μm steps from the surface (increasing depth from top left to bottom right). For F50NC50 treated samples, no fluorescence was detected below 30 to 40 μm from the surface, while fluorescence was detected up to 100 μm in depth for F50A samples. Scale bars are 50 μm.

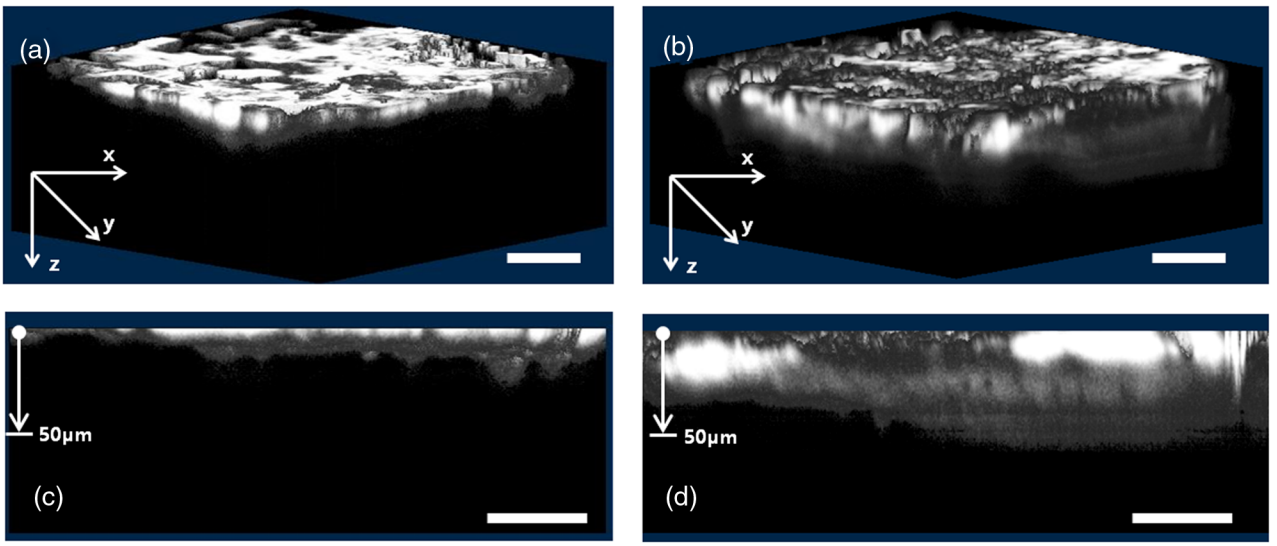

Fig. 6 Confocal Nile red fluorescence images of porcine skin samples. (a) Three-dimensional (3-D) render image of F50NC50 applied sample, (b) 3-D render image of F50A applied sample, (c) B-sectioned image of F50NC50 applied sample, and (d) XZ image of F50A applied sample. Scale bars are 50 μm.

z axis. Three-dimensional images visually confirm the previous result that F50A penetrated into the skin better than F50NC50. Since the porcine skin samples were treated with the same amount of nanoemulsions regardless of the type (F50A or F50NC50) and nonabsorbed amounts left on the surface were removed after 30 h of treatment, the spread and volume of pixels containing Nile red fluorescence signals imply the amount of transdermally delivered nanoemulsions into the skin. Only a fraction of F50NC50 nanoemulsion was found to be penetrated and mainly distributed near the skin surface, while a significantly larger amount of F50A nanoemulsion diffused well below the skin surface. Although further studies are needed to discriminate simple diffusion and proper internalization of nanoemulsions, asiaticoside loading clearly helped nanoemulsions penetrate deeper into the skin by targeting keratinocytes.

Although the previous three-dimensionally rendered images allow an intuitive visualization of the nanoemulsion distribution, the detection of Nile red fluorescence was limited up to 100 μm from the skin surface regardless of the presence of nanoemulsions. Therefore, the skin samples were sliced in the bottom-up direction, i.e., from the dermis to the epidermis direction to give 500-μm-thick slices for XZ Nile red fluorescence imaging to obtain a complete depth-direction distribution profile of nanoemulsions. If slices were be made in the top-down direction, a slicing blade could potentially carry nanoemulsions from the nanoemulsion-rich region (top, epidermis) to a less rich (bottom, dermis) region. This would cause an artificial enhancement of nanoemulsion absorption that should be avoided. Also, a clean, new surgical knife blade was used every time a cut was made to minimize contaminations with possible nanoemulsion residues left on the blade from the previous cutting operation.

Figure 7 shows XZ Nile red fluorescence images of the porcine skin samples cut in the depth direction with a surgical knife. Both images are of the size 300×300 μm^2. XZ Nile red fluorescence images also clearly show that the asiaticoside targeted nanoemulsion (F50A) penetrated deeper into the skin compared with the nontargeted nanoemulsion (F50NC50). While the F50A nanoemulsion had reached the basal layer as evidenced

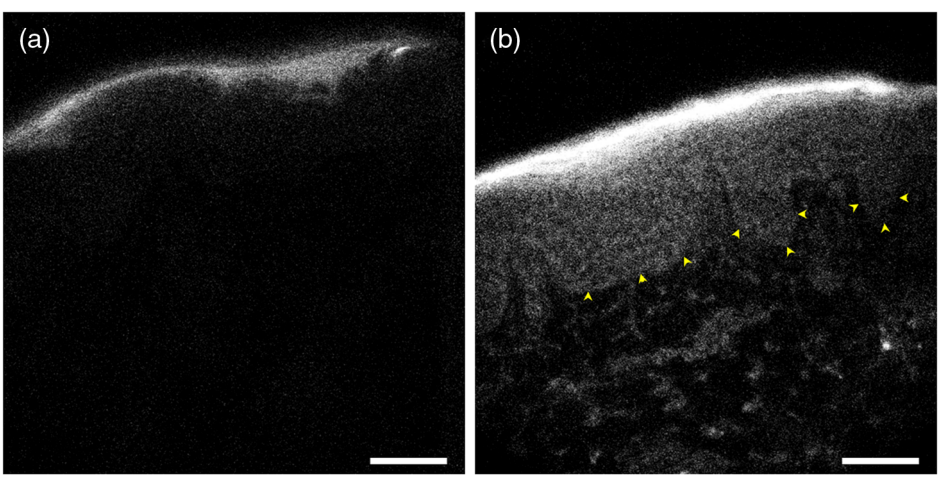

Fig. 7 XZ images of porcine skin samples applied with (a) F50NC50 and (b) F50A. Yellow arrows indicate the basal layer. Scale bars are 50 μm.

by scattered bright pixels, the F50NC50 nanoemulsion was not absorbed beyond the stratum corneum.

It is also important to note that the basal layer boundary is clearly visible in the case of the F50A applied skin. The epidermis is a cell-rich region composed of >90% keratinocytes, while the dermis is mainly composed of matrix components (collagen, elastin, extra fibrous matrix, etc.) and cells including fibroblasts, macrophages, and adipocytes. A denser distribution of F50A nanoemulsion as evidenced by brighter fluorescence on the epidermal side with respect to the boundary of the basal layer unequivocally demonstrates the self-targeting ability of asiaticoside-loaded nanoemulsion to selectively target keratinocytes.

4 Conclusion

In summary, we have successfully prepared *ex vivo* porcine skin samples and structural information was obtained by two-photon microscopy imaging. Then the porcine skin samples were treated with asiaticoside targeted (F50A) and nontargeted (F50NC50) nanoemulsions for 30 h. After the nanoemulsion treatment, Nile red fluorescence images revealing nanoemulsion distributions under the skin surface were acquired with CLSM. *En face* images, three-dimensional fluorescence images, and XZ images from the sliced samples all unambiguously reveal that F50A nanoemulsions penetrated deeper into the skin than F50NC50. Our result confirmed that the presence of specific target ligands on nanoemulsions can improve the binding affinity for keratinocyte cells resulting in better penetration into the *ex vivo* skin samples, and this improved nanoemulsion delivery can be potentially applied in many areas in cosmetics and drug delivery.

Acknowledgments

This study was supported by a grant of the Korean Health Technology R&D Project, Ministry of Health & Welfare, Republic of Korea (Grant No. HN12C0063) and by the National Research Foundation of Korea grant funded by the Korea government (MSIP) (No. 2008-0061891).

References

1. P. M. Elias, "Stratum corneum defensive functions: an integrated view," *J. Invest. Dermatol.* **20**(5), 183–200 (2005).
2. A. S. Michaels, S. K. Chadrasekaran, and J. E. Shaw, "Drug permeation through human skin: theory and in vitro experimental measurement," *AlChE J.* **21**(5), 985–996 (1975).
3. H. Sakurai, Y. Takahashi, and Y. Machida, "Influence of low-frequency massage device on transdermal absorption of ionic materials," *Int. J. Pharm.* **305**(1–2), 112–121 (2005).
4. I. Lavon and J. Kost, "Ultrasound and transdermal drug delivery," *Drug Discov. Today* **9**(15), 670–676 (2004).
5. K. Ng, "Enhancing transdermal drug delivery with low-frequency ultrasound," *Drug Discov. Today* **9**(21), 913 (2004).
6. M. B. Brown et al., "Dermal and transdermal drug delivery systems: current and future prospects," *Drug Deliv.* **13**(2), 175–187 (2006).
7. M. Haedersdal et al., "Fractional CO2 laser-assisted drug delivery," *Lasers Surg. Med.* **42**(2), 113–122 (2010).
8. M. R. Prausnitz, "Microneedles for transdermal drug delivery," *Adv. Drug Deliv. Rev.* **56**(5), 581–587 (2004).
9. A. Naik, Y. N. Kalia, and R. H. Guy, "Transdermal drug delivery: overcoming the skin's barrier function," *Pharm. Sci. Technol. Today* **3**(9), 318–326 (2000).
10. A. Kogan and N. Garti, "Microemulsions as transdermal drug delivery vehicles," *Adv. Colloid Interface Sci.* **123–126**, 369–385 (2006).
11. T. Delmas et al., "Nanoemulsion: preparation, stability and application in biosciences," in *Nanomaterials in Drug Delivery, Imaging, and Tissue Engineering*, A. Tiwari and A. Tiwari, Eds., pp. 1–55, John Wiley and Sons Inc., Hoboken, NJ (2013).
12. N. Atrux-Tallau et al., "Skin cell targeting with self-assembled ligand addressed nanoemulsion droplets," *Int. J. Cosmet. Sci.* **35**(3), 310–318 (2013).
13. M. Goutayer et al., "Tumor targeting of functionalized lipid nanoparticles: assessment by in vivo fluorescence imaging," *Eur. J. Pharm.* **75**(2), 137–147 (2010).
14. C. Qian and D. J. McClements, "Formation of nanoemulsions stabilized by model food-grade emulsifiers using high-pressure homogenization: factors affecting particle size," *Food Hydrocoll.* **25**(5), 1000–1008 (2011).
15. Y. Yuan et al., "Characterization and stability evaluation of β-carotene nanoemulsion prepared by high pressure homogenization under various emulsifying conditions," *Food Res. Int.* **41**(1), 61–68 (2008).
16. T. S. H. Leong et al., "Minimising oil droplet size using ultrasonic emulsification," *Ultrason. Sonochem.* **16**(6), 721–727 (2009).
17. S. Kentish et al., "The use of ultrasonics for nanoemulsion preparation," *Innov. Food Sci. Emerg. Technol.* **9**(2), 170–175 (2008).
18. S. M. Jafari, Y. He, and B. Bhandari, "Production of sub-micron emulsions by ultrasound and microfluidization techniques," *J. Food Eng.* **82**(4), 478–488 (2007).
19. P. Izquierdo et al., "Formation and stability of nano-emulsions prepared using the phase inversion temperature method," *Langmuir* **18**(1), 26–30 (2002).
20. P. Fernandeza et al., "Nano-emulsion formation by emulsion phase inversion," *Colloids Surf. A Physicochem. Eng. Asp.* **251**(1–3), 53–58 (2004).
21. J. Rao and D. J. McClements, "Stabilization of phase inversion temperature nanoemulsions by surfactant displacement," *J. Agric. Food Chem.* **58**(11), 7059–7066 (2010).
22. T. Trimaille et al., "Interfacial deposition of functionalized copolymers onto nanoemulsions produced by the solvent displacement method," *Colloid Polym. Sci.* **279**(8), 784–792 (2001).
23. V. C. F. Mosqueira et al., "Poly(D,L-lactide) nanocapsules prepared by a solvent displacement process: influence of the composition on physicochemical and structural properties," *J. Pharm. Sci.* **89**(5), 614–626 (2000).
24. A. Maestroa et al., "Influence of the phase behavior on the properties of ionic nanoemulsions prepared by the phase inversion composition method," *J. Colloid Interface Sci.* **327**(2), 433–439 (2008).
25. M. Hessien et al., "Stability and tunability of O/W nanoemulsions prepared by phase inversion composition," *Langmuir* **27**(6), 2299–2307 (2011).
26. P. Boukamp et al., "Normal keratinization in a spontaneously immortalized aneuploidy human keratinocyte cell line," *J. Cell Biol.* **106**(3), 761–771 (1988).

Biographies of the authors are not available.